

High Magnetic Field Induced Charge Density Wave State in a Quasi-One-Dimensional Organic Conductor

D. Graf,¹ E. S. Choi,¹ J. S. Brooks,¹ M. Matos,² R. T. Henriques,^{3,4} and M. Almeida⁴

¹NHMFL/Physics, Florida State University, Tallahassee, Florida 32310, USA

²Dept. de Engenharia Química, Instituto Superior de Engenharia de Lisboa, P-1900 Lisboa, Portugal

³Instituto de Telecomunicações, Instituto Superior Técnico, P-1049-001 Lisboa, Portugal

⁴Dept. de Química, Instituto Tecnológico e Nuclear, P-2686-953 Sacavém, Portugal

(Received 31 December 2003; published 13 August 2004)

The quasi-one-dimensional organic conductor $(\text{Per})_2\text{Pt}(\text{mnt})_2$ exhibits a charge density wave ground state below 8 K. Magnetoresistance and magnetization measurements show that the charge density wave is suppressed with magnetic fields of order 20 T, above which a high resistance state, with a cascade of subphases, appears. This new state, tentatively identified as a field induced charge density wave, reenters a low resistance state above 40 T. The results are presented in light of theoretical work [D. Zanchi *et al.* Phys. Rev. B **53**, 1240 (1996).] involving field induced charge density wave ground states in high magnetic fields.

DOI: 10.1103/PhysRevLett.93.076406

PACS numbers: 71.45.Lr, 72.15.Gd

The survival of broken symmetry singlet ground states in high magnetic fields, that would otherwise be Pauli-limited, is a subject of considerable interest. These ground states arise from electron-electron, or electron-hole pairing. In a simple quasi-one-dimensional (Q1D) conductor, single electron states with momentum difference of twice the Fermi wave vector ($2k_F$) near the Fermi level are involved. In finite magnetic fields, the Zeeman effect will shift k_F for each of the spin-up and spin-down bands. In Q1D, for both superconducting (SC) and spin density wave (SDW) systems, the spin-up – spin-down pairing momentum difference remains at $2k_F$ and hence both the SC and SDW states can survive in high magnetic fields. For superconductors, a SC state with electron pairs of finite total momentum is favored for magnetic fields near the Pauli limit, as described by the Fulde-Ferrell Larkin-Ovchinnikov formalism [1,2], and as recently reported for both organic[3,4] and intermetallic [5] layered superconductors. In the case of Q1D conductors, high magnetic fields can effectively suppress the interchain orbital motion, thereby driving the system more one-dimensional [6], and in many cases a field induced spin density wave (FISDW) state is stable for any further increases in magnetic field [7].

In contrast, for a charge density wave (CDW) ground state, with spin-up pairing (and spin-down pairing), the Zeeman shift of the bands will be $> 2k_F$ (and $< 2k_F$), which change continuously with increasing magnetic field. Hence a CDW state with a fixed nesting vector \mathbf{Q} will be destroyed for a Zeeman energy comparable to the CDW gap. [8] However, for a Q1D conductor with a CDW ground state, contributions from both spin and orbital coupling can allow the CDW \mathbf{Q} vector to adjust in field to produce an unconventional density wave state above the Pauli limit. The magnetic field dependence of CDW and field induced charged density wave (FICDW) states has been treated by Zanchi, Bjelis, and Montambaux

[9,10] (hereafter ZBM), Fujita *et al.*[11], McKenzie [12], and Lebed [13].

The ZBM model, which we will consider here, is an anisotropic two-dimensional Hamiltonian in the random phase approximation where both CDW and SDW correlations are included. Its predictions are as follows, using the notation x , y (or b in ZBM), and z to denote the intra-chain, interchain, and transverse crystal directions, with transfer integral parameters t_x , t_y (or t_b in ZBM), and t_z . The degree of imperfect nesting is given by $t'_y/t'_y^* \approx t'_y/T_c$ ($t'_y = 0$) where T_c is the CDW critical temperature, t'_y is the antinesting parameter, and t'_y^* is the value of the antinesting parameter which would destroy the CDW at zero field. The relative strength of the SDW and CDW coupling is given by $\nu = -U_s/U_c$, and $\eta = q_{\text{orbital}}/q_{\text{spin}} = eyv_F \cos\theta/\mu_B$ is a measure of the orbital effect in tilted magnetic fields away from the transverse direction. For $-1 \leq \nu \leq 1$, the CDW is favored. With increasing magnetic field, for $t'_y/t'_y^* \approx 0$, the CDW will be suppressed by the Pauli term, and the nesting vector \mathbf{Q} will remain constant (this is the CDW_0 state). However, irrespective of field direction, at a finite critical field H_{cx} the nesting vector will begin to shift ($\mathbf{Q} + \mathbf{q}_x$), and this will introduce a new state, CDW_x , which is a hybridized SDW-CDW state. For larger t'_y/t'_y^* , the zero field CDW transition temperature T_c^0 will decrease, even to zero for $t'_y/t'_y^* > 1$, but finite fields can restore the CDW. Hence for very poor nesting, the CDW state is actually field induced. In this regime, a cascade of FICDW transitions can be realized, but ultimately, in the high field limit, even the FICDW ground state is suppressed by the Pauli term. For $t_y \neq 0$, an intervening CDW_y ground state between CDW_0 and CDW_x can be stabilized at H_{cy} . CDW_y is a pure, nonhybridized CDW state which involves a transverse nesting vector change ($\mathbf{Q} + \mathbf{q}_y$).

Recent work by Andres, Kartsovnik, and co-workers has shown a correspondence between the ZBM predictions and the ground state of α -(BEDT-TTF)₂KHg(SCN)₄, expected to be a CDW resulting from QID nesting below $T_c \sim 8$ K (see Refs. [14–18]). The magnetic field dependence of the CDW transition temperature follows the CDW₀ to CDW_x scenario, pressure shows the influence of the antinesting parameter, and FICDW effects appear for strongly tilted magnetic fields. However, in addition to QID Fermi surface nesting, this compound also has a quasi-two-dimensional (Q2D) Fermi surface, making a comparison with theoretical predictions more complicated.

The QID conductor, (Per)₂Pt(mnt)₂ (where Per = perylene, mnt = maleonitriledithiolate and $T_c \sim 8$ K) also has a relatively low CDW transition temperature [19]. Comparison with FICDW theory should be more direct, since the structure is highly one-dimensional [$t_b(t_x) \approx 150$, $t_a(t_y) \approx 2$, and $t_c(t_z) \approx 0$ meV], with only a weak interchain bandwidth [20,21]. Recently, for the (Per)₂Au(mnt)₂ compound (with $T_c \sim 12$ K), suppression of the ambient CDW ground state above 30 T was observed, with evidence for a new high field induced state above 40 T suggestive of a FICDW [22,23]. For brevity, we refer the reader to these references for details. In (Per)₂Pt(mnt)₂, T_c is lower than in the $M = \text{Au}$ compound and based on the simple BCS and Clogston limit formalisms, we estimate the Pauli limit in this case to be around 15 T, which is consistent with our experimental findings. At higher fields, a high resistance state exhibiting sub-phases appears in the $M = \text{Pt}$ material, which is reentrant to a low resistance state above 40 T. Although the Pt ion has spin 1/2, we expect these spins to be completely aligned above 20 T. Hence, the high field behavior in (Per)₂Pt(mnt)₂ should be related only to the perylene conducting chains.

Samples of (Per)₂Pt(mnt)₂ were grown electrochemically [24]. Because of small sample size (1 mm × 50 μm × 25 μm), the a- and c-axis directions were difficult to determine, and x-ray data from previous studies on larger crystals was used to determine the crystal axes from visual comparisons. Sample resistance was measured with a four-terminal configuration with an a-c current of 1 mA along the b-axis of the samples. Torque magnetization involved a piezo-resistive cantilever [25] with a small (< 200 μg) (Per)₂Pt(mnt)₂ crystal attached to the sample arm. Measurements were made at NHMFL-Tallahassee in dc fields of 33 and 45 T using a rotating, low temperature sample stage.

The magnetoresistance of (Per)₂Pt(mnt)₂ below T_c^0 is shown in Fig. 1 for three different samples and field directions. At low fields, the divergent resistance is not measurable. With increasing field, the resistance decreases and approaches a low resistance value at a field B_0 near 20 T (at 0.5 K), where the ambient CDW (CDW₀) is suppressed. [In Fig. 1(b), we have indicated features in

the magnetoresistance that are common to most samples and orientations investigated.] Between B_0 and B_x , the resistivity is in the range 0.05 to 5 Ω – cm. Above B_x , a field induced high resistance state is entered, where step-like features in the magnetoresistance appear. Based on the predictions of ZBM, we tentatively identify this field induced high resistance state as a FICDW. Finally, above 40 T, the FICDW state is suppressed above a field B_e , and a new low resistance state is entered, which we have termed the high field state (HFS).

Referring to Fig. 1(c), the HFS resistance is still activated ($E_a \approx 30$ K at 45 T), although significantly less than at the center of the FICDW ($E_a \approx 80$ K at 32 T). The low resistance state between B_0 and B_x is also thermally activated ($E_a \approx 12$ K at 22 T), but becomes metallic for temperatures below 1 K. A small hysteresis was observed in the FICDW phase as shown in Fig. 1(c), where two additional slope changes are seen, one around 21 T at low temperatures, and one (labeled B_{d2} in Fig. 2(c)) between B_d and B_e . The very low resistance behavior seen in Fig. 1(c) below 1 K near 23 T was not observed in other samples.

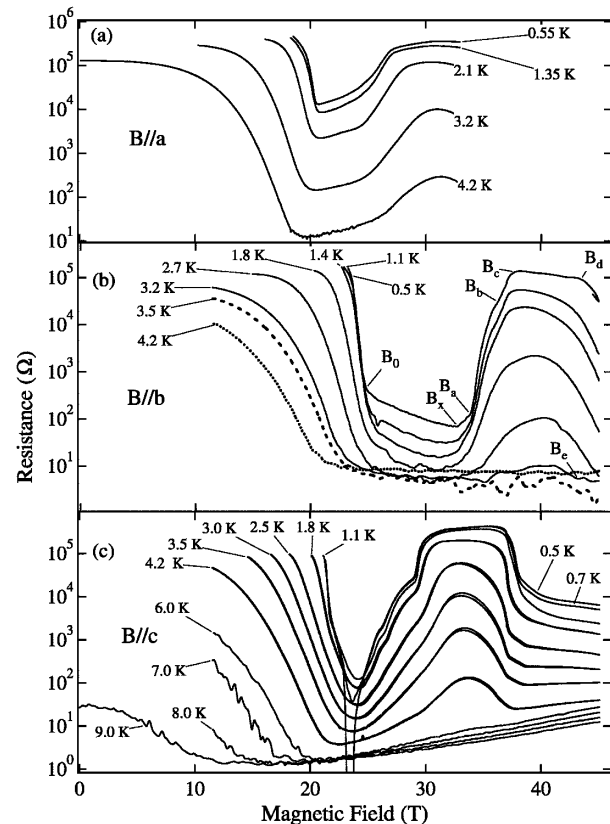


FIG. 1. (Per)₂Pt(mnt)₂ b-axis sample resistance vs. magnetic field for $T \leq T_c(0)$. (a) B//a for fields up to 33 T. (b) B//b to 45 T. Structures in the magnetoresistance common to all samples and field directions are labeled. (c) B//c to 45 T where additional structures in the magnetoresistance are observed (see text).

The phase diagrams for the CDW, FICDW, and HFS derived from the magnetoresistance data of Fig. 1 are shown in Fig. 2. The zero field transition temperatures were determined from the peaks in $\ln(R)/d(1/T)$ during the cool-down. Conventions defined in Fig. 1(b) demarcate common features that are independent of field direction. The temperature dependence of the subphase structure follows a positive slope below (solid symbols), and a negative slope above (open symbols) the center of the FICDW phase. Figures 1 and 2 show that the FICDW features do not obey a $1/\cos(\theta)$ dependence expected for a Q2D closed orbit Fermi surface.

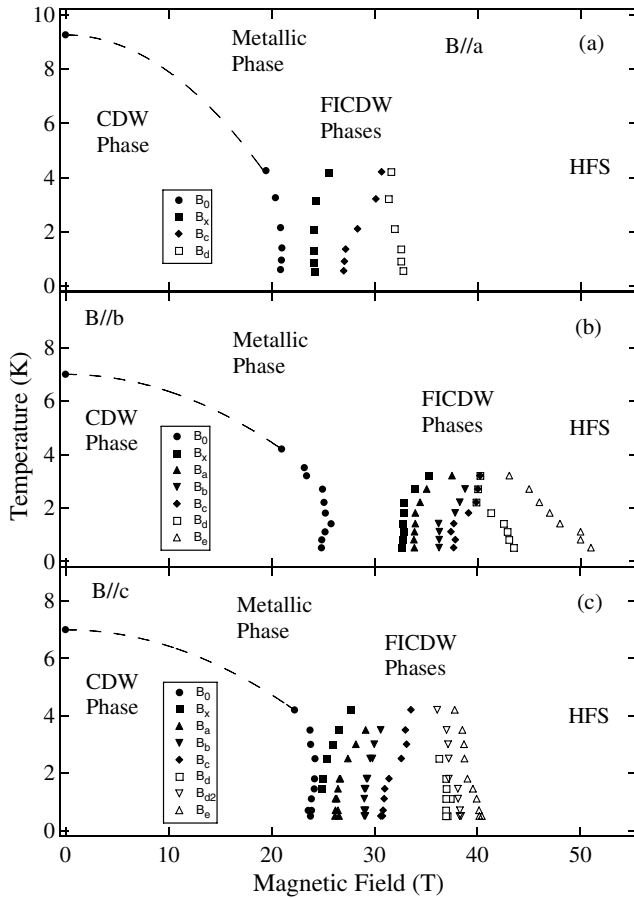


FIG. 2. Proposed T-B phase diagram of $(\text{Per})_2\text{Pt}(\text{mnt})_2$ based on the magnetoresistance studies in Fig. 1. Features of the magnetoresistance noted as B_o , B_x , and B_e indicate the suppression of the low field CDW state, the onset and termination of the FICDW state, respectively. Cascadelike properties of the magnetoresistance are identified as B_a , B_b , B_c , and B_d where closed symbols are below and open symbols are above the center of the FICDW. Dashed lines: quadratic extrapolation between $T_c(0)$ and $T_c(B_0)$. (a) B//a phase diagram based on Fig. 1(a). (b) B//b phase diagram based on Fig. 1(b). Note that the upper phase boundary B_e is an estimate based on a linear extrapolation of the data to fields above 45 T. (c) B//c phase diagram based on Fig. 1(c).

All angular dependent measurements (see also magnetization below) indicate that for the field parallel to the conducting chains (B//b) the transition fields (B_0 , B_x , etc.) attain the highest field values. However, for an increasing finite field component in the b-a or b-c planes, the transition fields are reduced, an effect we ascribe to the onset of orbital coupling. Orbital coupling in the a-b plane is possible since t_a is nonzero, but it is surprising that it is also present for the a-c plane, where t_c is virtually zero. Changes in the crystal structure at low temperatures could give rise to larger a and c bandwidths.

A thermodynamic investigation of the FICDW utilized torque (τ) magnetization measurements at 0.5 K for rotation in the a-c plane up to 33 T, as shown in Fig. 3, and for a rotation in the b-c plane to 45 T. Figure 3(a) shows selected magnetization signals (torque signal divided by magnetic field) for different sample orientations in the a-c plane. The sign and magnitude of the response is dependent on the sample and cantilever orientation, characteristic of the $\sin(2\theta)$ nature of the cantilever response [26]. Above the background we observe two peaks one and 2. Figure 3(b) shows sequential $|d^2\tau/dB^2|$ curves offset to reveal the angular dependences of the peaks, which are plotted in Fig. 3(c). Again, no $1/\cos(\theta)$ dependence is observed.

Qualitative similarities between the field induced state and theory suggest that it is a FICDW state, but the details of the $(\text{Per})_2\text{Pt}(\text{mnt})_2$ system do not directly follow. From band calculations [21], the antinesting parameter is $t'_y = t'_y/t'_x \approx 2^2/150 = 0.026$ meV, and the degree of antinesting, for $T_c = 8$ K, is $t'_y/t'_y^* \approx 0.038$. Hence for CDW_x , this puts $(\text{Per})_2\text{Pt}(\text{mnt})_2$ in the nearly perfectly nested limit. Assuming an effective mass of $1m_0$ and a quarter-filled band, the orbital impact parameter is $\eta = eyv_F \cos(\theta)/\mu_B \approx 7 \cos(\theta)$. These parameters of $(\text{Per})_2\text{Pt}(\text{mnt})_2$, predict no cascade since $t'_y/t'_y^* \ll 1$ (Ref. [9], Fig. 9), and that CDW_y is unlikely since $\eta > 2$ (Ref. [9], Figs. 4 and 7). We estimate the range of the reduced critical fields for field induced changes in nesting by taking the $B_0 \approx 20$ T field from Fig. 1 as H_{cx} . Then $h_{cx} = \mu_B H_{cx}/2\pi k_B T_c \approx 0.259$, within the range of the theory (Ref. [9], Fig. 2). The transverse critical field $h_{cy} = \mu_B H_{cy}/2\pi k_B T_c$ is between 0.3 and 0.425 (assuming it lies between B_0 and B_x). Although within the range of the theory, h_{cy} depends on η . For small η , $h_{cy} = 0.304(1 + 0.088\eta^2)^{1/2}$ and hence as the field is tilted into conducting x-y plane, H_{cy} decreases. In Fig. 3, it is apparent that for $(\text{Per})_2\text{Pt}(\text{mnt})_2$ all features associated with the FICDW increase as the in-plane field configuration (i.e. B//b) is approached.

Unlike the ZBM model where the CDW_0 and CDW_x phases are connected, our results show a gap between B_0 and B_x . For a greatly reduced interchain coupling as in the present case, the FICDW mechanism might be delayed after the CDW_0 state is destroyed. Then only when

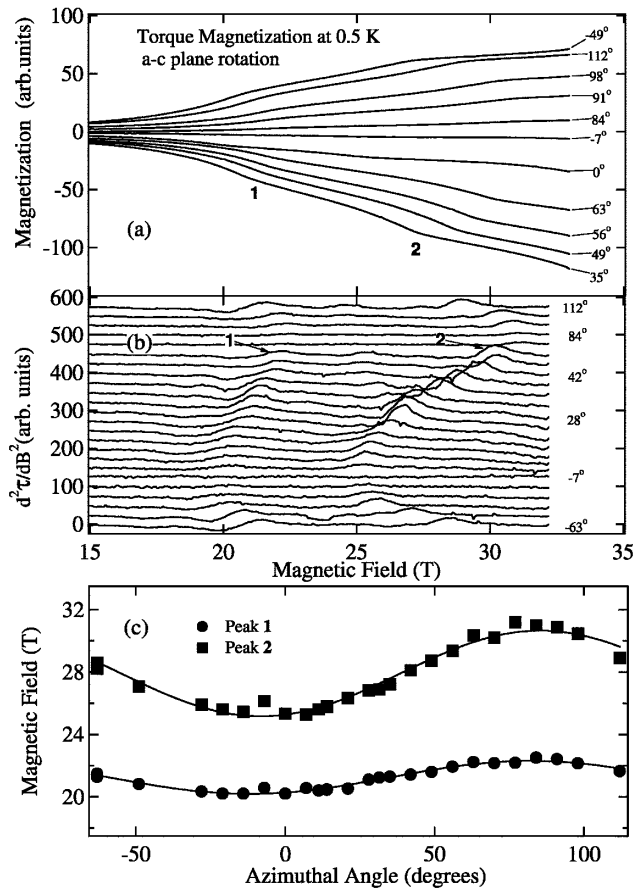


FIG. 3. Magnetization of $(\text{Per})_2\text{Pt}(\text{mnt})_2$ at 0.5 K up to 33 T. (a) Torque magnetization signal τ/B for a sample rotated in the a-c plane with respect the magnetic field. Transitions **1** and **2** in the field range 20 to 30 T are indicated. (b) The second derivative of the torque signal $|d^2\tau/dB^2|$ vs field and angle. (c) a-c plane angular dependence of the main magnetization signals **1** and **2**. Lines are sinusoidal fits to the data.

the orbital confinement induced by higher magnetic field finally can interact with the nearly QID system is the FICDW stabilized. In all but one measurement (near B_0 below 1 K in Fig. 2(c)), the low temperature resistance is activated over the entire phase diagram. This implies the presence of gapped states in addition to the CDW and the FICDW. This may be due to CDW-SDW hybridization predicted by ZBM, since the SDW ground state survives in high fields, as previously discussed.

Although there are qualitative comparisons with the ZBM model, it is possible that the high field states we report involves new physics, or modification of ZBM, where other mechanisms allow the nesting to either survive, or even to return. Since there are four donors per unit cell, the Fermi surface of $(\text{Per})_2\text{Pt}(\text{mnt})_2$ consists of four sheets, each with a small warping of ≈ 2 meV along the a-axis [21]. Through hybridization this topology may

allow small pockets, and therefore quantum oscillations, to exist. Likewise, for this band-splitting, a field of order 35 T could cause the spin-up band of one branch to overlap with the spin-down band of the other branch, resulting in a new well-defined nesting condition and the FICDW. In this case, upon further increase in field, the Zeeman splitting will eventually destroy the FICDW, as its field symmetric, reentrant nature suggests

This work is supported by NSF 02-03532, the NHMFL is supported by the National Science Foundation and the State of Florida, and DG acknowledges support from NSF GK-12. Work in Portugal is supported by FCT under Contract No. POCT/FAT/39115/2001. We are grateful to R. McKenzie for suggesting this experiment and to E. Canadell, M. Kartsovnik, A. Lebed, D. Zanchi, and K. Yang for helpful discussions.

- [1] A. I. Larkin and Y. N. Ovchinnikov, *Sov. Phys. JETP* **20**, 762 (1965).
- [2] P. Fulde and R. A. Ferrell, *Phys. Rev.* **135**, A550 (1964).
- [3] M. Houzet, A. Buzdin, L. Bulaevskii, and M. Maley, *Phys. Rev. Lett.* **88**, 227001 (2002).
- [4] H. Shimahara, *J. Phys. Soc. Jpn.* **71**, 1644 (2002).
- [5] H. A. Radovan, *et al.*, *Nature (London)* **425**, 51 (2003).
- [6] L. P. Gor'kov and A. G. Lebed, *J. Phys. (Paris) Lett.* **45**, L433 (1984).
- [7] T. Ishiguro, K. Yamaji and G. Saito, *Organic Superconductors II* (Springer-Verlag, New York, 1998).
- [8] W. Dieterich and P. Fulde, *Z. Phys.* **265**, 239 (1973).
- [9] D. Zanchi, A. Bjelis, and G. Montambaux, *Phys. Rev. B* **53**, 1240 (1996).
- [10] A. Bjelis, D. Zanchi, and G. Montambaux, *J. Physique IV (Paris)* **9**, 203 (1999).
- [11] M. Fujita, K. Machida, and H. Nakanishi, *J. Phys. Soc. Jpn.* **54**, 3820 (1985).
- [12] R. McKenzie, *cond-mat/9706235*, (1997).
- [13] A. G. Lebed, *JETP Lett.* **78**, 138 (2003).
- [14] D. Andres, *et al.*, *Phys. Rev. B* **64**, 161104(R) (2001).
- [15] D. Andres, *et al.*, *Synth. Met.* **120**, 841 (2001).
- [16] M. Kartsovnik, *et al.*, *Physica B* **346**, 268 (2004).
- [17] M. V. Kartsovnik, *et al.*, *J. Phys. IV (France)* **114**, 191 (2004).
- [18] D. Andres, *et al.*, *Phys. Rev. B* **68**, 201101 (2003).
- [19] M. Almeida and R. T. Henriques, in *Handbook of Organic Conductive Molecules and Polymers*, edited by H. Nalwa (Wiley, New York, 1997) Vol. 1, p. 110-114.
- [20] L. F. Veiros, M. J. Calhorda, and E. Canadell, *Inorg. Chem.* **33**, 4290 (1994).
- [21] E. Canadell (private communication).
- [22] D. Graf, *et al.*, *Phys. Rev. B* **69**, 125113 (2004).
- [23] R. D. McDonald, *et al.*, *cond-mat/0312142* (2003).
- [24] L. Alcacer, *et al.*, *Solid State Commun.* **35**, 945 (1980).
- [25] E. Ohmichi and T. Osada, *Rev. Sci. Instrum.* **73**, 3022 (2002).
- [26] V. G. Kogan, *Phys. Rev. B* **38**, 7049 (1988).